Vortex scaling ranges in two-dimensional turbulence

B. H. Burgess,[1, a)] D. G. Dritschel,[1] and R. K. Scott[1]

School of Mathematics and Statistics, University of St Andrews, St Andrews KY16 9SS, United Kingdom

(Dated: 6 November 2017)

[a)]Electronic mail: bhb3@st-andrews.ac.uk

We survey the role of coherent vortices in two-dimensional turbulence, including formation mechanisms, implications for classical similarity and inertial range theories, and characteristics of the vortex populations. We review early work on the spatial and temporal scaling properties of vortices in freely evolving turbulence, and more recent developments, including a spatiotemporal scaling theory for vortices in the forced inverse energy cascade. We emphasize that Kraichnan-Batchelor similarity theories and vortex scaling theories are best viewed as complementary, and together provide a more complete description of two-dimensional turbulence. In particular, similarity theory has a continued role in describing the weak filamentary sea between the vortices. Moreover, we locate both classical inertial and vortex scaling ranges within the broader framework of scaling in far-from-equilibrium systems, which generically exhibit multiple fixed point solutions with distinct scaling behaviour. We describe how stationary transport in a range of scales comoving with the dilatation of flow features, as measured by the growth in vortex area, constrains the vortex number density in both freely evolving and forced two-dimensional turbulence.

The new theories for coherent vortices reveal previously hidden nontrivial scaling, point to new dynamical understanding, and provide a novel exciting window into two-dimensional turbulence.

CONTENTS

I. INTRODUCTION

Coherent vortices form generically in both forced and freely evolving two-dimensional (2D) turbulence, merging and generating time-evolving spatial hierarchies distributed over a wide range of scales [1–7]. Neither Batchelor's similarity theory for freely evolving 2D turbulence[8] nor Kraichnan's inertial range theory for forced 2D turbulence[9] account for coherent vortices, and thus both incompletely describe turbulent flow. In particular, vortices introduce spatial intermittency and non-Gaussianity[10], interrupt cascade processes by trapping energy and enstrophy[11], and are associated with invariants, such as the peak vortex intensity[3,12], unaccounted for by Kraichnan-Batchelor theory.

Though they pose a challenge for traditional accounts of two-dimensional turbulence, vortices themselves are distributed across scales in power law ranges that can be modelled using concepts familiar from inertial range theory[7]. In fact, the energy and enstrophy cascades of Kraichnan-Batchelor theory and the vortex scaling ranges of both freely evolving and forced turbulence all fit together within the broader framework of far-from-equilibrium systems, which exhibit multiple scaling ranges with distinct power law behaviour. These scaling ranges are associated with non-thermal fixed points and with stationary transport of conserved quantities across scales[13]. In the direct and inverse cascades enstrophy and energy are transported through spectral space; the counterpart of this in vortex scaling ranges is transport of conserved quantities defined on the vortex subfield across scales in vortex area space by interactions between vortices[7,14].

In this article we review the important role played by coherent vortices in 2D turbulence and the scaling theories that have been developed to describe vortex populations in both forced and freely evolving flows. Section II covers coherent vortex formation, the effect vortices have on scaling and implications for the validity of similarity theories, as well as the partition between the weak filamentary sea and intense long-lived vortices in both the forced and freely evolving systems. Section III describes the relationship between inertial range theory and spatiotemporal vortex scaling theories, and introduces key concepts. Scaling theories for vortices in freely evolving 2D turbulence and the forced inverse energy cascade are described in sections III A and III B, respectively, and section III C covers generalizations of these theories to scale-dependent and time-varying vortex intensities. In section IV we summarize our current understanding of vortex scaling ranges in 2D turbulence and some

directions for further research.

II. VORTICES AND SIMILARITY THEORY

Freely evolving 2D turbulence started from random-phase fields with power at all scales develops spatial hierarchies of vortices[1,2,5,15,16]. These coherent structures originate in the initial vorticity field as localized intense concentrations, which merge, partially axisymmetrize, and develop into well-defined vortices that persist for time scales much longer than the enstrophy transfer time $Z^{-1/2}$[1,17,18], where $Z \equiv \frac{1}{2\mathcal{D}} \int \omega^2 d\mathbf{x}$ is the enstrophy per unit area, with $\omega = -\nabla^2\psi$ the vorticity and ψ the streamfunction. Here, $\mathcal{D}$ is the area of a finite region large enough that the statistics converge.

We illustrate the process of vortex formation and growth in figures 1a–1c, which show vorticity fields from a direct numerical simulation (DNS) of freely evolving 2D turbulence starting from an initial energy spectrum $\mathcal{E}(k) \sim e^{-(k-k_0)^2/\sigma^2}$, where $k_0 = 512$ and $\sigma = 50$. The resolution is 8192^2 and the fields are shown on a 384^2 subdomain. Extrema in the initial field (figure 1a) evolve into weakly elliptical coherent vortices, which can be seen in figure 1b. Less intense fluctuations between the vortices are strained into filaments, cascading enstrophy to smaller scales[17], leaving essentially only the vortices at late times, as evident in figure 1c.

Batchelor's similarity theory for freely evolving two-dimensional turbulence assumes that all enstrophy is involved in the cascade, such that in the long-time inviscid limit energy E is the only invariant and a similarity state with

$$\mathcal{E}(k) = E^{3/2} t g(\sqrt{E} k t), \tag{1}$$

where g is a universal function and $E \equiv \frac{1}{2\mathcal{D}} \int \psi\omega d\mathbf{x}$ is the energy, is established independent of initial conditions[8]. Coherent vortices, however, trap enstrophy and protect it from the cascade, breaking the similarity assumption of Batchelor's theory[16,17,19,20]. As a result[1,18] the observed energy spectrum is significantly steeper than k^{-3}.

The situation is similar in the forced inverse energy cascade, where the vorticity field is sensitive to forcing and dissipation, and coherent vortices form by a variety of distinct mechanisms[7,10,21–25]. As just discussed in the context of freely evolving two-dimensional turbulence, vortices arise from localized concentrations in the forcing field. This formation

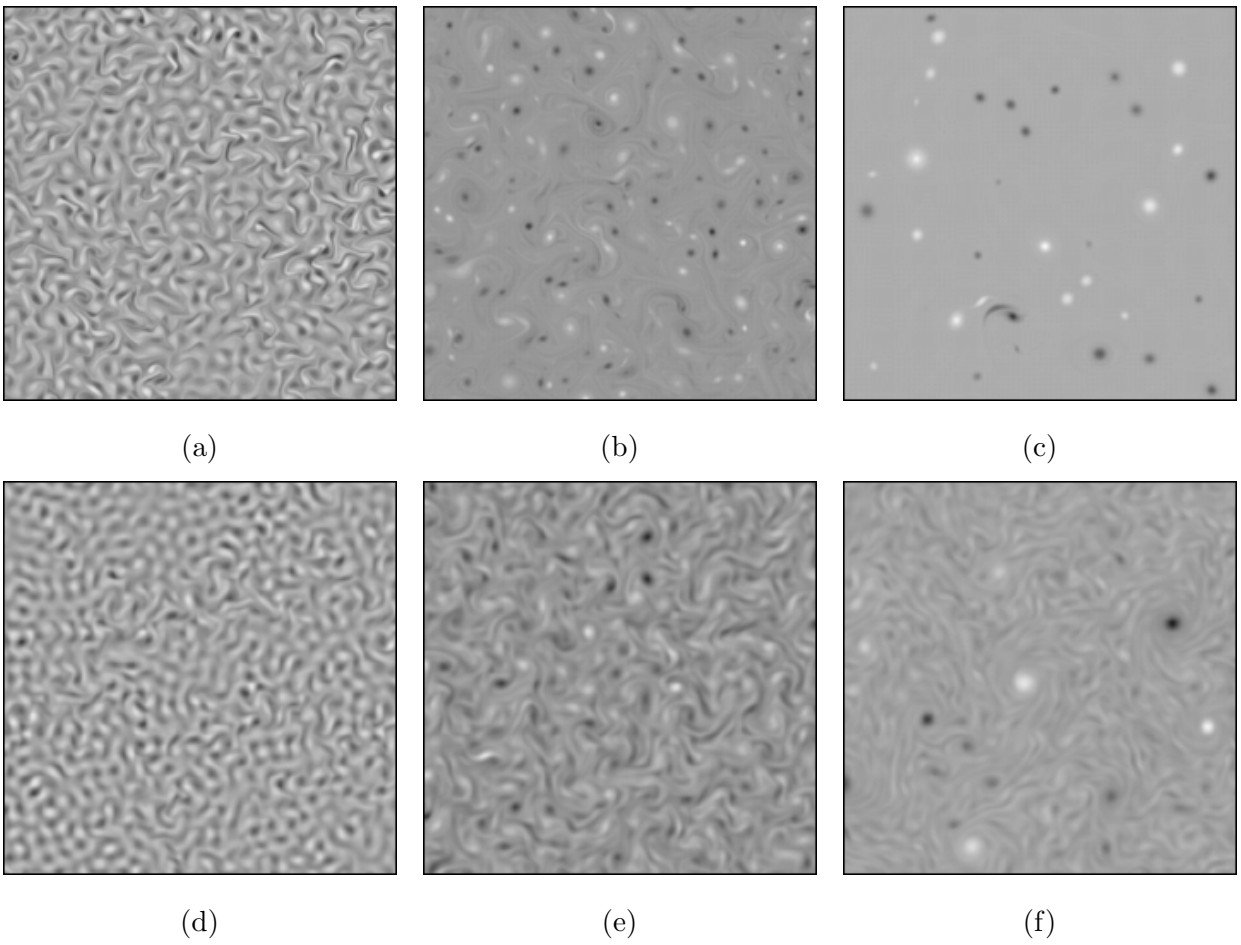

FIG. 1: (a)-(c) Vorticity fields from DNS of freely evolving turbulence starting from an initial energy spectrum $\mathcal{E}(k) \sim e^{-(k-k_0)^2/\sigma^2}$, where $k_0 = 512$ and $\sigma = 50$, shown on a 384^2 subdomain at nondimensional times $t/T_\omega = 4$, 41, and 347, left to right, where $T_\omega = 4\pi/\omega_{\rm rms}(0)$ is an eddy turnover time and $\omega_{\rm rms}(0)$ is the rms vorticity of the initial vorticity field. (d)-(f) Vorticity fields from a forced inverse cascade with narrow-band δ-correlated forcing at wavenumber $k_f = 1024$, shown on a 192^2 subdomain at nondimensional times $t/T_E = 9$, 19, and 187, left to right, where $T_E = (\varepsilon k_f^2)^{-1/3}$, with ε the energy flux to large scales.

mechanism is evident in figure 1d, which shows the Gaussian forcing at the onset of nonlinear self-advection, when localized regions in the random vorticity field are beginning to shear and strain into filamentary structures. In panel 1e, small vortices have formed from forcing field extrema; these vortices grow through merger, generating a population distributed across scales, as shown in figure 1f. Vortex formation by this mechanism occurs for both narrow-band and broadband spatially random forcing, independent of forcing bandwidth, forcing

correlation time, and order of viscosity[25].

Another vortex formation mechanism observed in the forced two-dimensional inverse cascade is aggregation of anomalously intense vorticity regions, shown in figure 2; this occurs in flows forced near the dissipation wavenumber, with small forcing Reynolds number[25]. These flows have initially amorphous vorticity fields lacking both intense weakly elliptical coherent vortices and the filamentary structures associated with the enstrophy cascade. Nevertheless, using a threshold on vorticity one can still identify vorticity anomalies – regions of intense vorticity concentration that lack the circular shape of coherent vortices seen in simulations forced at larger scales. As shown in figure 2 (bottom row), the like-sign anomalies so-identified cluster together. This suggests an aggregation process in which anomalies cluster, merge, and eventually form the intense weakly elliptical coherent vortices visible in the right panels. Thus the inverse energy cascade has a robust tendency to form coherent vortices, even when the forcing Reynolds number is low. This formation mechanism again has a parallel in freely evolving 2D turbulence, where patches of vorticity aggregate, culminating in inelastic collisions between well-defined coherent vortices[1].

In both forced and freely evolving two-dimensional turbulence coherent vortices coexist with an incoherent filamentary sea, but the partition between the coherent and background vorticity and its time evolution differ. In the freely evolving system the enstrophy decay rate grows and peaks at early times. As the flow evolves, filaments in the sea are stretched out, becoming increasingly passive, and cascade their enstrophy to smaller scales. At late times, the filamentary sea has all but disappeared, leaving only the coherent vortices, which contain almost all the energy and control the dynamics, including the enstrophy decay rate, since only filaments shed during vortex mergers are now available to participate in the enstrophy cascade. The progressive disappearance of the filamentary sea and persistence of coherent vortices can be seen in figures 1a–1c.

In forced two-dimensional turbulence, on the other hand, the incoherent intervortex flow is continuously replenished, compensating loss to dissipation; background vorticity levels thus do not decay exponentially but equilibrate at a finite level, which is nonetheless much lower than that found within the coherent vortices, where enstrophy is protected starting at early times from dissipative decay. In this case strong, nearly-circular coherent vortices can again be unambiguously distinguished from the weak filamentary background flow[6,7,10,21–24].

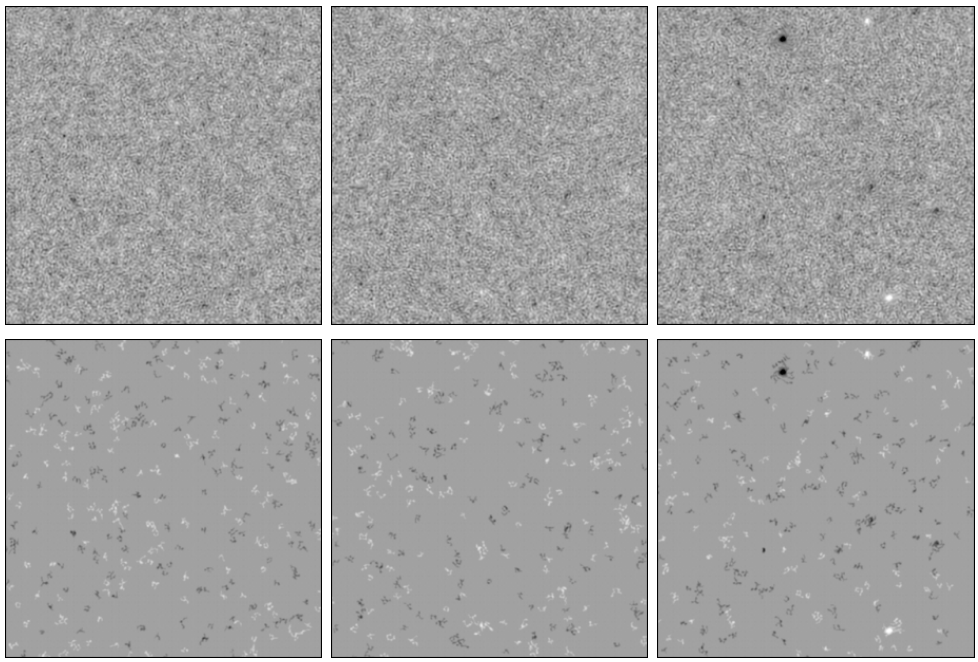

FIG. 2: Total vorticity (top) and anomaly (bottom) fields from an inverse cascade simulated by Burgess & Scott[25] at resolution 8192^2 with narrow-band δ-correlated forcing at wavenumber $k_f = 2048$ and 4^{th}-order hyperviscosity. The subdomain is 384^2 grid points, corresponding to side length $96 l_f$, where l_f is the forcing length scale. The nondimensional times are $t/T_E = 183$, 276, and 577, left to right, where $T_E = (\varepsilon k_f^2)^{-1/3}$, with ε the energy flux to large scales. The data is from a simulation discussed in B. H. Burgess and R. K. Scott, "Robustness of vortex populations in the two-dimensional inverse energy cascade," *J. Fluid Mech.* (Submitted).

The persistance of the incoherent filamentary sea in the forced system and its disappearance in the freely evolving system can been seen by comparing the top and bottom panels in figure 1. In both systems, populations of long-lived weakly elliptical vortices emerge from spatially random initial conditions, from either the initial vorticity field in freely evolving turbulence or from the forcing field in forced turbulence, as evident in figures 1c and 1f, though the properties of the vortex populations differ, as will be discussed in section III.

Though vortices alter the scaling of globally integrated quantities, steepening the energy spectrum and introducing intermittency, continuous wavelet analysis shows that in the forced inverse cascade the incoherent flow in regions sufficiently far from the vortices approximately satisfies Kraichnan's inertial range theory[10]. Vortices are first identified as regions exceeding a threshold on vorticity, and the field over which the wavelet spectrogram is computed is

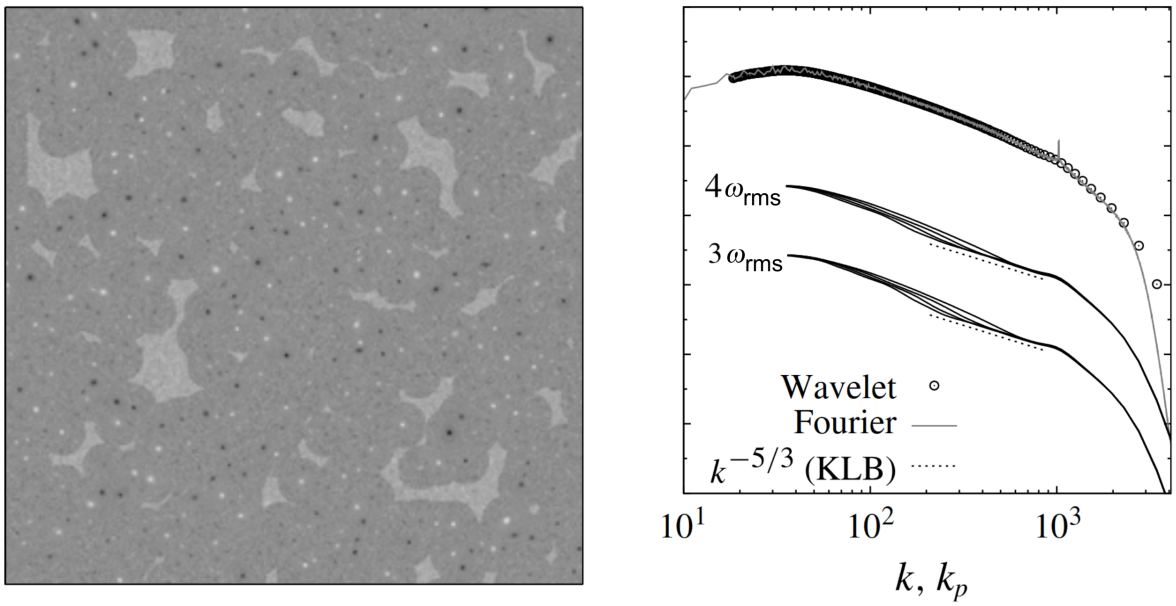

(a) (b)

FIG. 3: (a) Vorticity field with light regions over which the wavelet spectrogram is computed and (b) wavelet and Fourier spectra for the total vorticity field and light regions as selected by two choices of vorticity threshold, $3\omega_{\rm rms}$ and $4\omega_{\rm rms}$, as indicated. For each value of the threshold, we show spectrograms corresponding to four increasing (top to bottom) minimum distances from vortices, with $k^{-5/3}$ scaling for comparison. Figures are reprinted with permission from Burgess *et al.*[10], copyright © 2015 by Cambridge University Press.

restricted to subdomains, such as the light areas shown in figure 3a, sufficiently far from vortices. The resulting spectrogram contains a range in which $\mathcal{E}(k) \sim k^{-5/3}$, as predicted by Kraichnan[9], and this range extends to larger scales as the minimum allowed distance to vortices increases, as is evident from examining the middle and lower sets of black curves in figure 3b: these spectra correspond, from top to bottom, to increasing minimum distances to vortices. Similarly, Fontane *et al.*[6] found $\mathcal{E}(k) \sim k^{-2}$ for the entire vorticity field, but $\mathcal{E}(k) \sim k^{-5/3}$ for the incoherent part, using a entirely different vortex extraction method. Thus, despite the impact of coherent vortices on globally integrated properties, Kraichnan inertial range theory has a continued role in describing the inverse cascade sufficiently far from vortices.

III. INERTIAL RANGE THEORY AND VORTEX SCALING RANGES

The dominance of coherent vortices at late times in freely evolving two-dimensional turbulence and their robust formation in the inverse energy cascade mean that any account of two-dimensional turbulence is incomplete without theories for these vortex populations. In both flows vortices grow through merger and populate a wide and growing range of scales, indicating that ultimately theories must describe temporally evolving spatial hierachies.

Systems far from equilibrium generically exhibit multiple scaling ranges with distinct power laws at different scales, each range associated with a fixed point and stationary transport of a conserved, or approximately conserved, quantity[13]. The dual cascades of Kraichnan inertial range theory are a canonical example, in which the transported quantities are enstrophy and energy in the direct and inverse cascades respectively[9].

Given the generic occurence of such scaling ranges in far from equilibrium systems, it is natural to develop a theory for the vortex populations of 2D turbulence within this framework. Burgess & Scott[7] first applied these ideas to the forced inverse energy cascade, extending inertial range arguments to the vortex subfield, with transport across scales in vortex area space mediated by interactions between vortices taking the place of transport through wavenumber space.

We begin our discussion of vortex scaling theories by introducing some basic concepts. We then review early theories for vortices in freely evolving 2D turbulence, and the spatiotemporal theory of Dritschel *et al.*[5], showing how the concept of stationary transport applies in that system. In section III B we discuss the theory recently developed by Burgess & Scott for vortices in the forced inverse energy cascade[7]. We conclude our discussion of vortex scaling theories by considering in section III C generalizations to scale- and time-dependent vortex intensities.

Two key assumptions in Kraichnan's seminal theory of inertial ranges in two-dimensional turbulence are self-similar scaling of the energy spectrum $\mathcal{E}(ak)/\mathcal{E}(k) = a^{-m}$ and triple correlation function $T(ak, ap, aq)/T(k, p, q) = a^{-(1+3m)/2}$, and k-independent energy and enstrophy fluxes. In combination these two constraints fix the energy spectral scaling exponents at $m = 5/3$ in the inverse energy cascade and $m = 3$ in the direct enstrophy cascade. Self-similarity and k-independent flux, i.e. stationary transport of a conserved quantity, are generically associated with fixed point solutions. With this in mind, we also combine these

ingredients to constrain the spatial and temporal scaling exponents of the number density distribution of vortices $n(A)$ as a function of vortex area A, which we assume takes the power law form

$$n(A,t) = c(t)A^{-r_i} \sim t^{\alpha_i}A^{-r_i}, \qquad i \in 1, ..., S, \tag{2}$$

where $c(t) \sim t^{\alpha_i}$ has dimensions A^{r_i-1} and S is the number of scaling ranges. Here, the number density is normalized such that $n(A)dA$ is the number of vortices having areas between A and $A + dA$.

An immediate question is how to define the area A of a vortex. Coherent structure identification is complicated, and there does not at present exist an agreed-upon definition of a coherent vortex, though two widely-accepted requirements are that vortices are concentrated regions of intense vorticity, and that they propagate with a high degree of material invariance[26]. In defining vortex areas A, we wish to choose regions that describe the flow in a way likely to yield new insight into turbulent dynamics. With this in mind, there are theoretical reasons to expect vorticity isolines and their enclosed regions to be especially significant in the description of two-dimensional turbulence. For example, the approach of contour dynamics relies on the fact that the equations of motion for an incompressible Eulerian fluid can be formulated in terms of vorticity isolines[27]. Furthermore, considering two-dimensional incompressible fluids, Virasoro (1981) derives an action principle in which the canonical coordinates are isovorticity lines, with 'vorticity densities' as the conjugate momenta[28]. These theoretical considerations motivate our definition of a vortex as a region of intense vorticity enclosed by a vorticity isoline, i.e. the vortex boundary is a level set of vorticity. The support of the region is the area A, and we define the intensity of the vortex as the mean square vorticity evaluated over its area A. The extraction method reflecting these theoretical considerations, and therefore appropriate to the theory, is then a threshold on vorticity.

Three candidate conserved quantities potentially associated with A-independent flux through area space in distinct scaling ranges are the first three moments of $\overline{\omega_{\rm v}^2}n(A)$,

$$E_{\rm v} = \tfrac{1}{2\mathcal{D}} \int \overline{\omega_{\rm v}^2}A^2 n(A)dA, \tag{3}$$

$$Z_{\rm v} = \tfrac{1}{2\mathcal{D}} \int \overline{\omega_{\rm v}^2}An(A)dA, \tag{4}$$

$$\sigma_{\rm v} = \tfrac{1}{2\mathcal{D}} \int \overline{\omega_{\rm v}^2}n(A)dA. \tag{5}$$

Here $\mathcal{D}$ is the area of a region large enough that the statistics have converged, and $\overline{\omega_{\rm v}^2}$ is the vortex intensity, or mean square vorticity evaluated over vortices of area A,

$$\overline{\omega_{\rm v}^2(A)} \equiv \frac{1}{N}\sum_{i=1}^{N}\frac{1}{A_i}\int_{A_i}\omega^2 d\mathbf{x}, \tag{6}$$

where $A_i \in [A - dA, A + dA]$, i.e. the sum is taken over all vortices whose areas lie within a bin centered on A, and N is the total number of such vortices. In practice these bins are the same as those used to compute the number density. We will define the integration limits for equations (3)–(5) shortly. The first two quantities are the vortex energy $E_{\rm v}$ and vortex enstrophy per unit area $Z_{\rm v}$, given in equations (3)–(4) respectively, and we interpret the third quantity, $\sigma_{\rm v}$, given in (5) as an intensity-weighted vortex number, or 'charge density'. If $\overline{\omega_{\rm v}^2}$ is independent of A and t, then conservation of $\sigma_{\rm v}$ is equivalent to conservation of vortex number,

$$N_{\rm v} = \int n(A) dA. \tag{7}$$

The question now arises as to the appropriate A-space interval in which to enforce conservation, i.e. what the integration limits should be in equations (3)–(5) and (7). Firstly, we note that in both freely evolving 2D turbulence and the forced inverse cascade there is a dilatation of length scales associated with flow features growing larger in size. With this in mind we borrow from cosmology the concept of a 'comoving frame', i.e. a frame comoving with the expansion of the universe[29]. We apply this concept in A-space by considering a range of scales that grows along with the dilatation of flow features. More specifically, we define a 'comoving' interval $[\mu A_0(t), A_0(t)]$, where $0 < \mu < 1$ is a constant, which has endpoints that evolve with the growth in vortex area. Any value may be chosen for μ as long as $\mu A_0(t)$ and $A_0(t)$ fall within the same scaling range. It is in comoving intervals that we will enforce conservation: this is motivated by the expectation that certain features of the system should be invariant under the dilatation associated with the flow evolution. Which features are invariant, and, relatedly, which quantities are conserved, will depend on the particular scaling range in question.

We note that individually vortices may jump from scale to scale and even decrease in size as a result of mergers, rather than increasing in size steadily[30]. However, we can picture an average 'statistical vortex' as increasing in size continually at the vortex growth rate. In a comoving interval one imagines following such a statistical vortex as it grows in area,

moving through A-space toward larger scales. We assume that statistical vortices in all scaling ranges grow at the same rate, which can be derived using similarity arguments in both the forced and freely evolving systems. This assumption amounts to using the vortex growth as a measure of the dilatation and assuming that a single time-dependent dilatation factor is relevant to understanding the number density at all scales.

Unlike energy E and enstrophy Z in the familiar Kraichnan-Batchelor inertial range theories, there are no exact flux form conservation laws for the flow of $E_{\rm v}$, $Z_{\rm v}$, and $\sigma_{\rm v}$ past a given A. Nonetheless, we will still find scaling ranges in $n(A,t)$ associated with local conservation of $E_{\rm v}$, $Z_{\rm v}$, and $\sigma_{\rm v}$ despite the fact that these quantities are not globally conserved. Similar situations arise in other nonequilibrium systems, where scaling ranges associated with local conservation are seen despite the fact that the theory does not exactly conserve the quantity. For example, relativistic quantum field theories that have particle number changing processes can nonetheless exhibit approximate particle number conservation in weak wave turbulence scaling regimes[13].

A. Scaling theories for vortices in freely evolving two-dimensional turbulence

The earliest vortex scaling theories for freely evolving 2D turbulence treated the spatial and temporal aspects of the population separately. Benzi *et al.*[1] linked the scaling of the energy spectrum to a hierarchical population of self-similar vortices with an algebraic number density $n(R) \sim R^{-\alpha}$, where R is vortex radius. A measured value $\alpha = 1.9$ yielded $\mathcal{E}(k) \sim k^{-4.1}$, close to their observed spectrum $\mathcal{E}(k) \sim k^{-4.3}$. In addition, they predicted $\alpha = 2$ based on energy-conserving mergers, but assumed an equilibrated state, in which $n(R)$ had no overall time dependence. Carnevale *et al.*[3] and Weiss & McWilliams[4] took the opposite approach, developing a 'mean-vortex' theory for a dilute vortex gas consisting of N vortices with average radius r_a and vorticity amplitude ζ_a. Assuming that energy $E \sim N\zeta_a^2 r_a^2$ and the vorticity amplitude ζ_a were conserved, and that the vortex number evolved algebraically, $N(t) = N(t_0)(t/t_0)^{-\xi}$, they obtained $r_a(t) = r_a(t_0)(t/t_0)^{\xi/4}$, and measured $\xi = 0.75$ from numerical simulations. Subsequent studies[2,4,11,31–38] found values that ranged from $\xi = 0.44$[32] to $\xi = 1$[36], though most were close to $\xi \approx 0.7$. A number of theories were proposed to predict ξ, including ballistic aggregation[35,39,40], a Coulomb gas model[41], and mean field models[36,42,43]. Lacasce[44] linked the decay of the vortex density to dispersion, and showed that, given the

measured mean vortex area growth rate, the density decay rate could be predicted from a scaling relation involving the collision time.

Since the vortex population observed in freely evolving 2D turbulence is neither time-invariant nor characterised by a single scale, Dritschel *et al.*[5] set out to unify the spatial and temporal scaling theories. In their theory, vortices are assumed to contain almost all the energy E, and the vortex intensity $\overline{\omega_{\rm v}^2}$ is taken to be independent of vortex area A and time t. The number density is thought of as having only one scaling range, and the exponent is fixed by requiring a scale-invariant distribution of vortex areas, such that

$$n(A) = c(t)A^{-1}. \tag{8}$$

The energy scales in the same way as the vortex energy defined in equation (3),

$$E \sim E_{\rm v} = \frac{1}{2\mathcal{D}} \int_{\mu A_0}^{A_0} \overline{\omega_{\rm v}^2} A^2 n(A) dA \sim c(t) A_0^2. \tag{9}$$

Energy conservation implies

$$c(t) \sim A_0^{-2}, \tag{10}$$

and in turn vortex number and enstrophy scale as

$$N_{\rm v} \sim A_0^{-2}, \qquad\qquad Z_{\rm v} \sim A_0^{-1}, \tag{11}$$

which follows from substituting equations (10) and (8) into (7) and (4).

The theory is closed by relating the growth rate of the area of a statistical vortex to the rate $dZ_{\rm v}/dt$ at which enstrophy is transferred to filaments. These rates are naturally linked because both vortex growth and processes such as filament ejection and vortex destruction, which lead to enstrophy dissipation, occur as a result of vortex interactions. Self-similarity is again a key ingredient: enstrophy per unit area $\overline{\omega_{\rm v}^2} A n(A) dA$ is required to decay at a scale-invariant rate, which is assumed proportional to the collision probability $p_{\rm col}$, the enstrophy $Z_{\rm v}$, and inversely proportional to the interaction time $T_{\rm int}$,

$$\frac{dZ_{\rm v}}{dt} \sim -p_{\rm col} \frac{Z_{\rm v}}{T_{\rm int}}. \tag{12}$$

Now, the collision probability is proportional to the vortex number density, $p_{\rm col} \sim c \sim A_0^{-2}$, where we have used equation (10). The interaction time $T_{\rm int} = r/U_{\rm v}$ measures the time a vortex travelling at speed $U_{\rm v}$ takes to travel a distance $r \sim (1/N_{\rm v})^{1/2} \sim c^{-1/2} \sim A_0$, where

r is the characteristic intervortex distance of vortices with areas A between μA_0 and A_0. The speed U_v is taken to be constant, an assumption verified in our simulations, where translational vortex speeds depend only weakly on vortex area, as shown in figure 4c for a pseudospectral simulation labelled Tophat-PS (simulation details given below). We thus have $T_\mathrm{int} = r/U_\mathrm{v} \sim A_0$. Substituting $Z_\mathrm{v} \sim A^{-1}$, $p_\mathrm{col} \sim A^{-2}$, and $T_\mathrm{int} \sim A$ (where we have renamed A_0 to A) into (12), one obtains

$$A^{-2} dA/dt \sim A^{-4}, \tag{13}$$

which implies

$$A(t) \sim t^{1/3}. \tag{14}$$

Vortex number and enstrophy then follow the decay laws,

$$N_\mathrm{v} \sim t^{-2/3}, \qquad Z_\mathrm{v} \sim t^{-1/3}, \tag{15}$$

obtained by substituting $A_0 \sim t^{1/3}$ into (11). Substituting the vortex area growth law into equation (10) one arrives at the prediction

$$n(A) \sim t^{-2/3} A^{-1}. \tag{16}$$

Sample number densities and vortex intensities from freely evolving 2D turbulence are shown at three times compensated by $t^{2/3}$ (upper gray curves) in figure 4. The stage of the flow evolution in the freely evolving simulations discussed here and below in section III C is given in terms of the dimensionless time

$$\tau = t/T_\omega, \tag{17}$$

where $T_\omega = 4\pi/\omega_\mathrm{rms}(0)$ is an eddy turnover time and $\omega_\mathrm{rms}(0)$ is the rms vorticity of the initial vorticity field. In panel (a) the densities are from a contour advection (CA) simulation performed by the Combined Lagrangian Advection Method (CLAM)[45] on a 2048^2 basic inversion grid, with effective resolution $(16 \cdot 2048)^2 = 32,768^2$; the initial energy spectrum is centered on $k_0 = 64$ with $\mathcal{E}(k)$ constant for $k \in [26.5, 101.5]$. In panels (b) and (c) the densities are from a standard pseudospectral (PS) simulation at resolution 8192^2 with fourth-order hyperviscosity; the initial energy spectrum is centered on $k_0 = 512$ and constant for

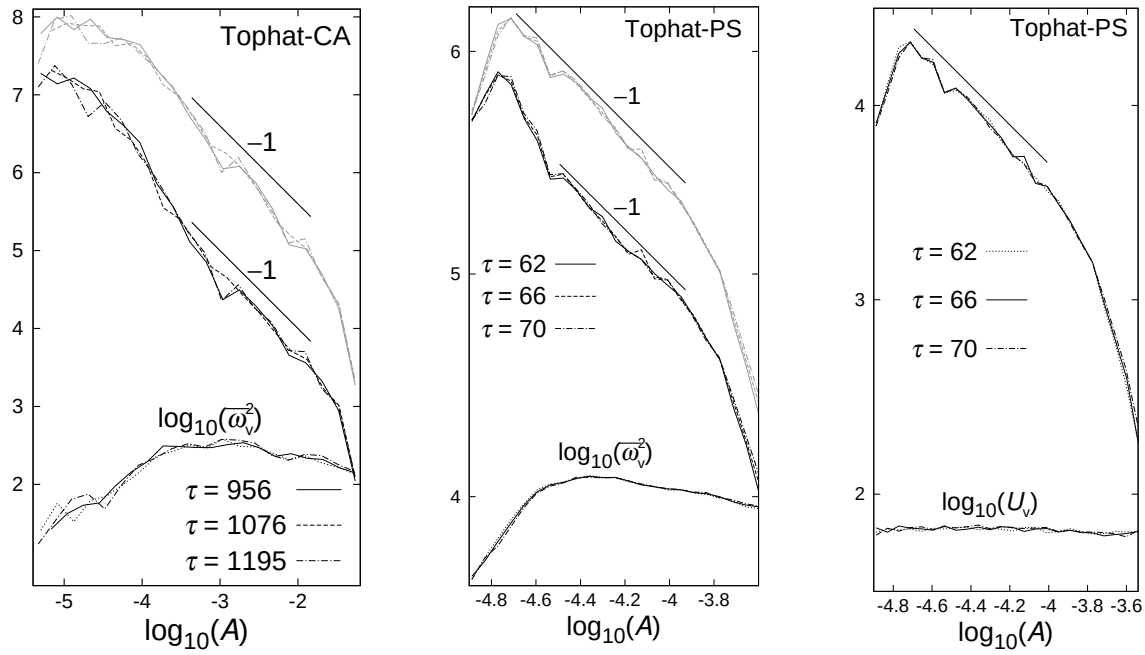

(a) (b) (c)

FIG. 4: Vortex intensities $\log_{10}[\overline{\omega_{\rm v}^2}(A,t)]$ and compensated number densities $\log_{10}[t^{2/3}n(A)]$ (upper gray curves) and $\log_{10}[t^{2/3}n(A)/\overline{\omega_{\rm v}^2}]$ (lower black curves) from simulations (a) Tophat-CA and (b) Tophat-PS[14] at three times with -1 slope (solid black line) for comparison. The slopes of the ranges spanned by the -1 line are (a) -1.14 ± 0.05 (gray) and -1.06 ± 0.03 (black) and (b) -1.13 ± 0.02 (gray) and -0.99 ± 0.02 (black). The densities and intensities are shifted for clarity of presentation. (c) Normalized number densities $\log_{10}[n(A)/N]$, where N is the total number of vortices, and vortex translational speeds $\log_{10}(U_{\rm v})$ for simulation Tophat-PS at three times with -1 slope (solid black line) for comparison. Data is from simulations discussed in Burgess *et al.*,"Extended scale invariance in the vortices of freely evolving two-dimensional turbulence," Phys. Rev. Fluids (Submitted).

$k \in [212, 812]$. The simulations are labelled Tophat-CA and Tophat-PS, respectively, where Tophat refers to the shape of the initial energy spectrum. For these initial conditions, $n(A)$ approximately follows the scaling A^{-1}, with the closest agreement at the small-scale end of the number density in simulation Tophat-PS (right panel), though the slope is somewhat steeper than the prediction of equation (16) in both simulations. We will discuss the modified scaling shown in the black curves in section III C below.

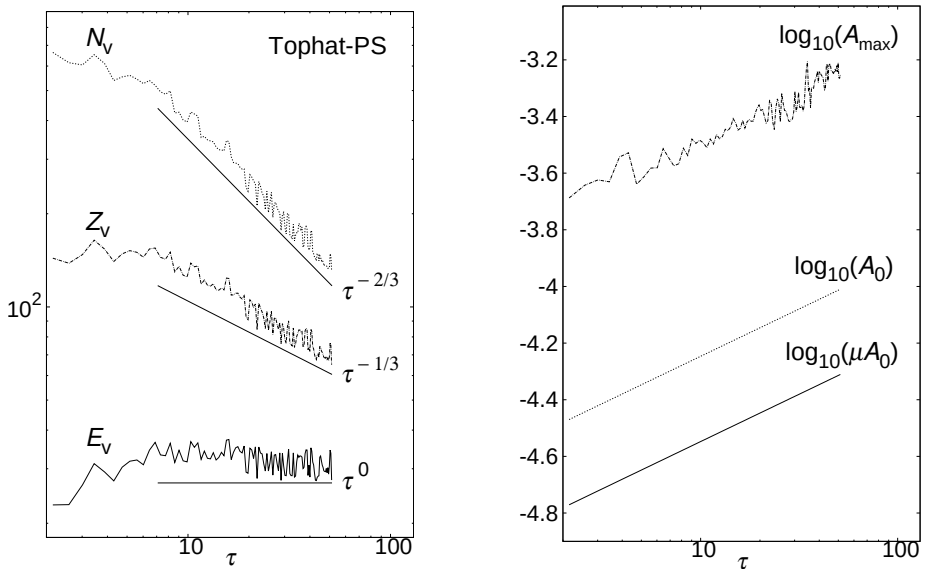

(a) (b)

FIG. 5: (a) N_v (dotted), Z_v (dash-dot), and E_v (solid) for the A^{-1} range; (b) endpoints of the corresponding comoving interval $[\mu A_0(\tau), A_0(\tau)]$ and area $A_{\max}$ of the largest vortex. Data is from a simulation discussed in Burgess *et al.*, "Extended scale invariance in the vortices of freely evolving two-dimensional turbulence," Phys. Rev. Fluids (Submitted).

Figure 5a shows the time evolution of vortex energy $E_{\rm v}$, vortex enstrophy per unit area $Z_{\rm v}$, and vortex number $N_{\rm v}$ as functions of nondimensional time τ for simulation Tophat-PS in a comoving interval $[\mu A_0(\tau), A_0(\tau)]$, whose endpoints are shown in 5b, together with the area $A_{\max}$ of the largest vortex. Comparing with figure 4b, shows that $\mu A_0(\tau)$ and $A_0(\tau)$ both fall within the approximate A^{-1} scaling range. Vortex energy $E_{\rm v}$ is conserved, and $N_{\rm v}$ and $Z_{\rm v}$ follow the predicted decay laws given in equation (15).

B. Forced inverse cascade

There has long been evidence for the presence of vortices in the forced inverse energy cascade of two-dimensional turbulence[21–24], but appreciation for the complex hierarchical structure of these populations is much more recent[6,7,10]. Fontane *et al.*[6] studied the vortex number density in forced two-dimensional turbulence and found a transition of the scaling at $k \approx k_f$, where k_f is the forcing wavenumber. However, there was insufficient range between the forcing and domain scale to draw any firm conclusions.

As discussed above, vortices form and grow in the forced inverse energy cascade via the same mechanisms observed in freely evolving two-dimensional turbulence, namely persistence of intense vorticity concentrations arising in the initial field, aggregation, and merger processes. However there are some important differences between freely evolving 2D turbulence and the forced inverse energy cascade. One difference is the presence of an additional scale in the problem, namely the forcing scale, which suggests immediately that the number density will have a more complex structure with at least one additional range. Secondly, unlike freely evolving 2D turbulence the forced inverse energy cascade involves an incoherent intervortex flow containing substantial amounts of energy and enstrophy, which is replenished by the forcing, as shown in figure 1d–1f. This incoherent flow interacts with the vortices and may modify their dynamics. It is natural to expect that these differences will be reflected in the dynamics and scaling of the vortex population.

Taking into account the presence of the forcing scale and an equilibrated incoherent intervortex flow, Burgess & Scott[7] formulated a scaling theory for vortices in the inverse energy cascade with energy injected at a constant rate, such that $E \sim t$. They postulated that a scale-invariant distribution of vortex areas, as seen in the freely evolving system, would also be found in the forced system far enough away from the forcing scale and the largest vortex. The continuous effect of forcing, especially on smaller-scale structures in the inverse cascade, suggests an additional range located between the forcing and the scale-invariant area distribution. Likewise, the largest vortex introduces a scale that disrupts self-similarity, suggesting a third range between the upper end of the scale-invariant area distribution and the largest vortex. These considerations lead to a minimal picture of a three-part vortex number density,

$$n(A,t) = c(t)A^{-r_i} \sim t^{\alpha_i}A^{-r_i}, \qquad i \in 1,2,3. \tag{18}$$

A schematic number density is shown in figure 6 with ranges (1)-(3) labelled, along with the characteristic forcing-scale vortex area A_f, maximum vortex area $A_{\max}$, and transition regions A_- and A_+ demarcating the intermediate scale-invariant range (2).

To proceed with the theory, a prediction is needed for the vortex area growth law. To obtain this, we consider the dimensionless combination

$$k\sqrt{4E/Z}, \tag{19}$$

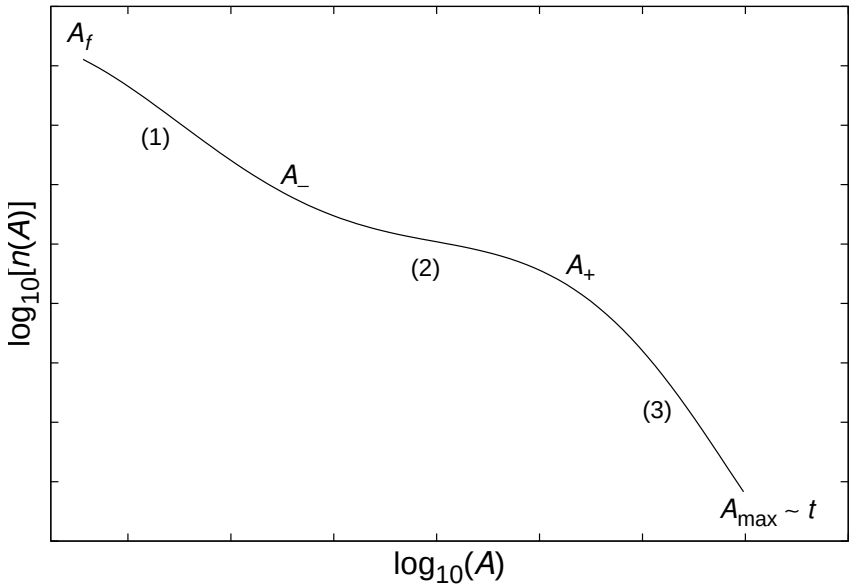

FIG. 6: Schematic of a three-part number density $n(A)$, with forcing-scale area A_f, transitional areas A_- and A_+, and maximum vortex area $A_{\max}$ labelled. Data is from a simulation discussed in Burgess *et al.*, "Extended scale invariance in the vortices of freely evolving two-dimensional turbulence," Phys. Rev. Fluids (Submitted).

where $k \equiv 2\pi/l$ is the wavenumber associated with length scale l and $1/\sqrt{Z}$ is an eddy turnover time. Enstrophy can neither increase nor decrease in the inverse cascade, where we expect vanishing enstrophy flux; hence, $Z =$ constant. Substituting this and $E \sim t$ into (19) we obtain

$$l_\omega \equiv 2\sqrt{4E/Z} \sim t^{1/2}. \tag{20}$$

This length scale can be associated with a vortex core as follows: noting that intense vortices dominate the velocity field[1], we identify the tangential speed of the vortex core with $u = \sqrt{2E}$. Relating this tangential speed to the angular velocity $\sqrt{2Z}/2$ then yields the prediction $d = l_\omega = 2\sqrt{4E/Z}$ for the vortex diameter. In turn, this yields a vortex area growth law

$$A \sim l_\omega^2 \sim t. \tag{21}$$

This is much faster than the $A(t) \sim t^{1/3}$ growth law found in freely evolving two-dimensional turbulence[5], and most likely reflects a higher merger rate in the forced system.

We now discuss the three proposed scaling regimes depicted in figure 6. Range (1) extends over the scales $A_f < A < A_-$; it is 'pinned' at one end to the forcing scale A_f and we imagine

it to be equilibrated with the forcing, which injects energy at a constant rate. Because this range is equilibrated, $\sigma_{\rm v}$, $N_{\rm v}$, $Z_{\rm v}$, and $E_{\rm v}$ will all be constant in the fixed interval $[\mu A_1, A_1]$, where A_1 does not vary in time and again $0 < \mu < 1$ is a constant factor. This conservation requirement sets $\alpha_1 = 0$. We also postulate that $E_{\rm v}$ will be conserved in a comoving interval, $[\mu A_0(t), A_0(t)]$, where $A_0(t) \sim t$. This is analogous to k-independent energy flux through energy-cascading subranges in two dimensional turbulence, except that here we are working in A-space, and the flux is restricted to the vortex subfield. Conservation of $E_{\rm v}$ implies $r_1 = 3$, such that $n(A) \sim A^{-3}$ and

$$E_{\rm v} = \frac{1}{2\mathcal{D}} \int_{\mu A_0(t)}^{A_0(t)} \overline{\omega_{\rm v}^2} A^2 n(A) dA \sim \int_{\mu A_0(t)}^{A_0(t)} A^{-1} dA \sim -\log \mu \sim t^0. \tag{22}$$

Using $A_0(t) \sim t$ and assuming $\overline{\omega_{\rm v}^2}$ is constant, it follows that

$$Z_{\rm v} \sim t^{-1}, \qquad N_{\rm v} \sim t^{-2}. \tag{23}$$

The intermediate scaling regime (2) extends over the range $A_- < A < A_+$. A self-similar distribution of vortex areas in this range again constrains the number density $n(A) \sim A^{-1}$. In the forced system we expect enstrophy lost to filament shedding during merger to be replaced, so that $Z_{\rm v}$ remains constant,

$$Z_{\rm v} = \frac{1}{2\mathcal{D}} \int_{\mu A_0(t)}^{A_0(t)} \overline{\omega_{\rm v}^2} A n(A) dA \sim c(t) \overline{\omega_{\rm v}^2} A_0(t) \sim t^0, \tag{24}$$

Substituting in $A_0(t) \sim t$ and again assuming that $\overline{\omega_{\rm v}^2}$ is constant in time, we obtain

$$c(t) \sim t^{-1}. \tag{25}$$

Equations (3) and (7) in turn yield

$$E_{\rm v} \sim t, \qquad N_{\rm v} \sim t^{-1}. \tag{26}$$

The predicted $c(t) \sim t^{-1}$ decay of the vortex density is also faster than the $c(t) \sim t^{-2/3}$ found for freely evolving turbulence[5]. Again, the difference most likely reflects a higher vortex merger rate.

In regime (3) vortices populate new and larger scales. We imagine that the vortices, which are spaced far apart, merge with other large vortices only rarely, such that the number of

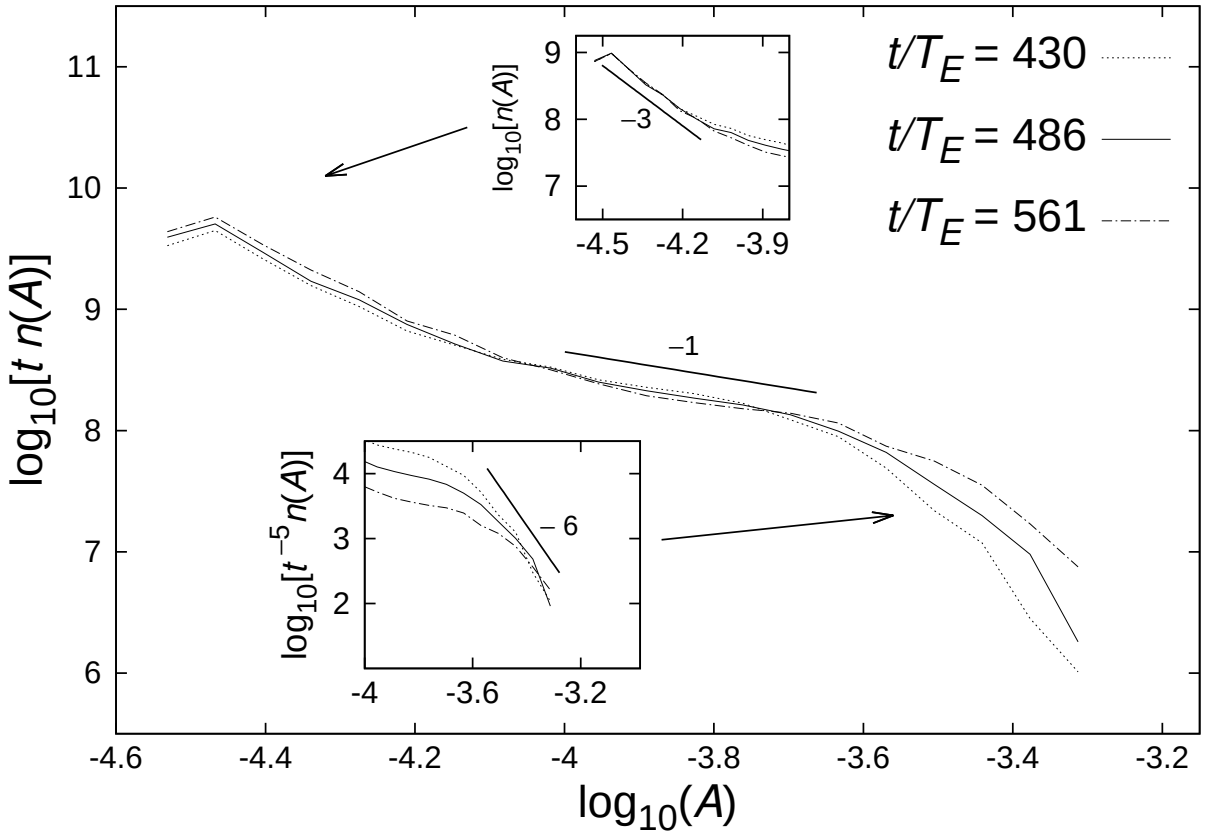

(a)

FIG. 7: Number density $n(A)$ compensated by t (main panel), uncompensated thermal bath (upper inset), and large-scale front compensated by t^{-5} (lower inset). The densities are shown at nondimensional times t/T_E, where $T_E = (\varepsilon k_f^2)^{-1/3}$ is a characteristic time based on the enstrophy injection rate, and ε is the constant energy flux to large scales. Figure reprinted with permission from Burgess & Scott[7], copyright © 2017 Cambridge University Press.

vortices N_v in a comoving interval $[\mu A_0(t), A_0(t)]$ remains constant. Substituting (18) into (7) and integrating then gives the condition $\alpha_3 = r_3 - 1$. From conservation of N_v it also follows that

$$E_\mathrm{v} \sim t^2, \qquad Z_\mathrm{v} \sim t. \tag{27}$$

Because of the lower merger rate within range (3), we expect enhanced occupation numbers, resulting in a steeper slope than in the intermediate range.

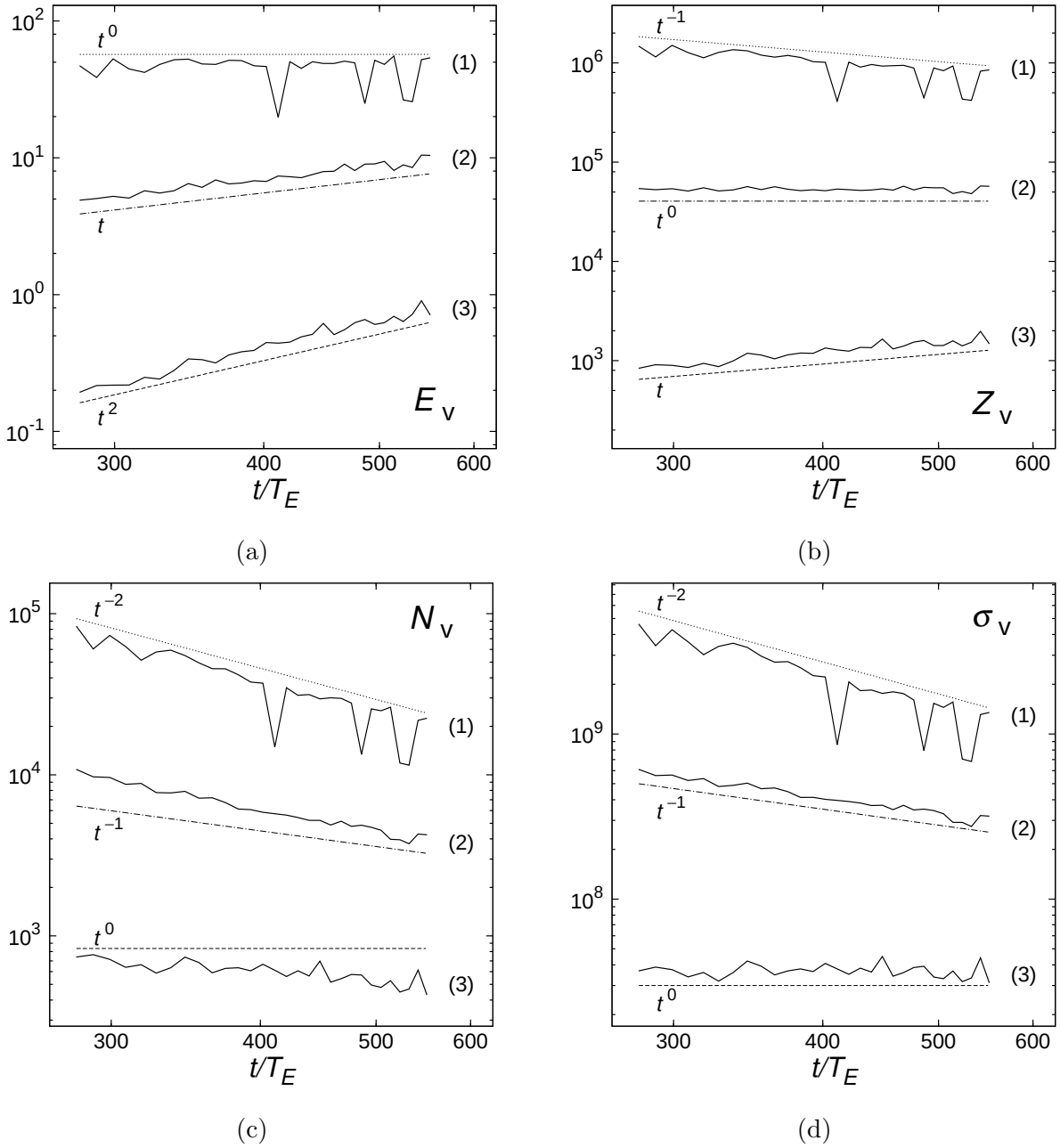

FIG. 8: (a) $E_{\rm v}$, (b) $Z_{\rm v}$, (c) $N_{\rm v}$, and (d) $\sigma_{\rm v}$ integrated over comoving intervals in ranges (1), (2), and (3), with slope lines for comparison, all plotted as functions of the nondimensional time t/T_E, where $T_E = (\varepsilon k_f^2)^{-1/3}$. Figures reprinted with permission from Burgess & Scott[7], copyright © 2017 Cambridge University Press.

In summary, we predict a vortex number density of the form

$$n(A,t) \sim \begin{cases} A^{-3}, & A_f \leq A < A_-, \\ t^{-1}A^{-1}, & A_- < A < A_+, \\ t^{r_3-1}A^{-r_3}, & A_+ < A \leq A_{\max}, \end{cases} \tag{28}$$

where A_- and A_+ are time-evolving transitional vortex areas. Matching the number densities at A_- and A_+ yields

$$A_- \sim t^{1/2}, \qquad A_+ \sim t^{r_3/(r_3-1)}. \tag{29}$$

Figure 7 shows $n(A)$ compensated by t (main panel), uncompensated in the thermal bath range (1) (upper inset), and compensated by t^{-5} in the large-scale front range (3) (lower inset). There are three distinct regimes, and the prediction of equation (28) is well satisfied, though the collapse is not perfect in range (2). The scaling in range (3) suggests $r_3 = 6$, such that $n(A) \sim t^5 A^{-6}$, though the evidence for a power law and collapse of the curves is weakest in this range. In section III C we will explore modifications to equation (28) following from allowing $\overline{\omega_\mathrm{v}^2}$ to depend on A and t.

Figures 8a–8b show the evolution of the vortex energy E_v and vortex enstrophy Z_v defined in equations (3) and (4), respectively. These quantities are integrated over comoving intervals falling within ranges (1), (2), and (3). In range (1) the vortex energy is conserved, and in range (2) the vortex enstrophy is conserved, as predicted. We will discuss the vortex number N_v and intensity-weighted vortex number σ_v in section III C.

C. The effect of time-varying area-dependent vortex intensities

The theories of Dritschel *et al.*[5] and Burgess & Scott[7] both assume that vortex intensities $\overline{\omega_\mathrm{v}^2}$ are uniform in A and time-invariant. In this section we discuss the scaling of the number density when $\overline{\omega_\mathrm{v}^2}(A,t)$ is non-uniform in A and/or time-dependent.

Forced inverse cascade

Beginning with the forced inverse cascade, we allow $\overline{\omega_\mathrm{v}^2} = \overline{\omega_\mathrm{v}^2}(A,t)$ to depend on A and t and require conservation of E_v and Z_v to continue holding in ranges (1) and (2). We note

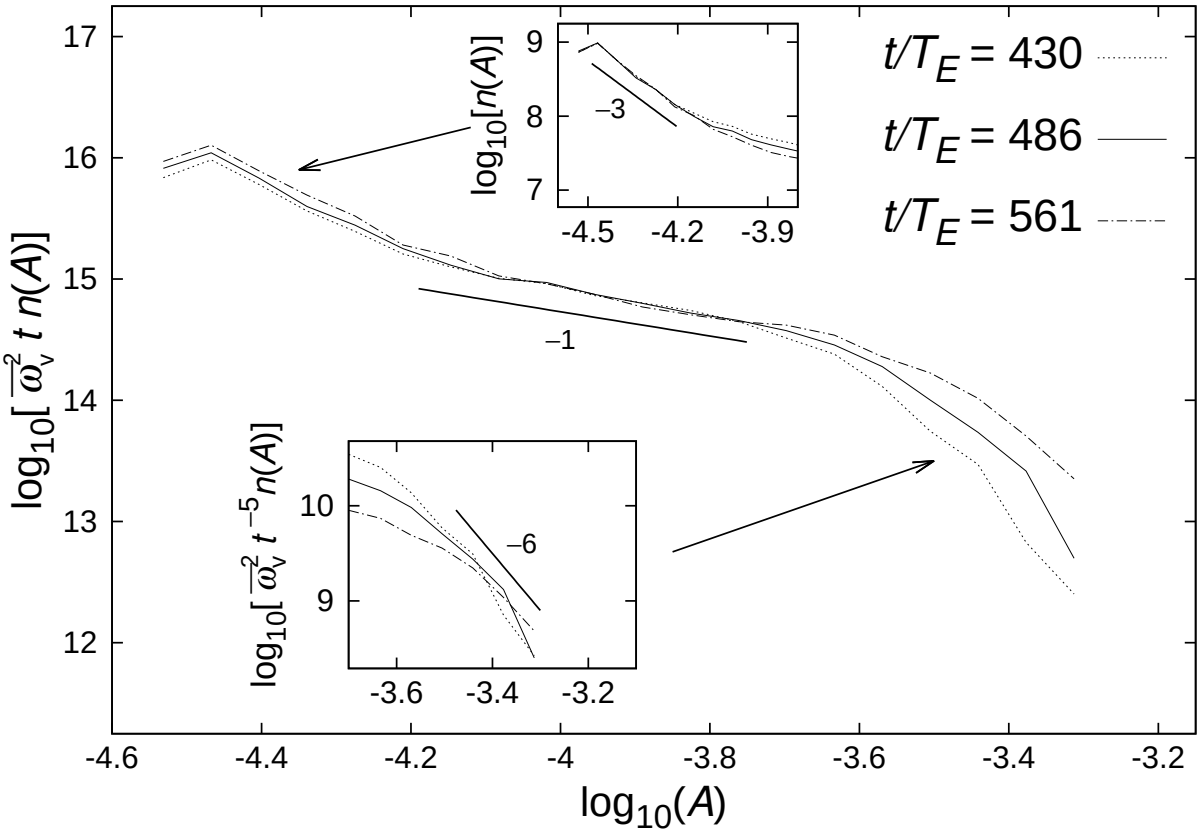

(a)

FIG. 9: Number density $n(A)$ compensated by $\overline{\omega_{\rm v}^2}t$ (main panel), uncompensated thermal bath (upper inset), and large-scale front compensated by $\overline{\omega_{\rm v}^2}t^{-5}$ (lower inset). The densities are shown at nondimensional times t/T_E, where $T_E = (\varepsilon k_f^2)^{-1/3}$.

that conservation of vortex number $N_{\rm v}$ is no longer equivalent to conservation of $\sigma_{\rm v}$ since $\overline{\omega_{\rm v}^2}$ is not constant, and we now hypothesize that $\sigma_{\rm v}$ will be conserved in range (3). Similar scaling arguments to those above give a modified three part number density[7]:

$$n(A,t) \sim \begin{cases} A^{-3}, & A_f \le A < A_-, \\ \overline{\omega_{\rm v}^2}^{-1} t^{-1} A^{-1}, & A_- < A < A_+, \\ \overline{\omega_{\rm v}^2}^{-1} t^{r_3-1} A^{-r_3}, & A_+ < A \le A_{\rm max}. \end{cases} \tag{30}$$

Allowing $\overline{\omega_{\rm v}^2}$ to evolve differently in ranges (2) and (3) gives transitional areas[7]

$$A_- \sim (\overline{\omega_{\rm v}^2})_2^{1/2} t^{1/2}, \qquad A_+ \sim \left[\frac{(\overline{\omega_{\rm v}^2})_2}{(\overline{\omega_{\rm v}^2})_3}\right]^{1/(r_3-1)} t^{r_3/(r_3-1)}, \tag{31}$$

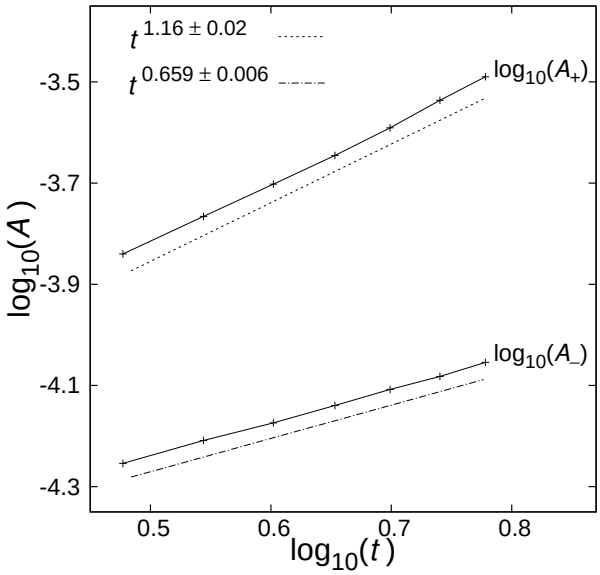

FIG. 10: Transitional areas A_- and A_+ together with best fit lines. Figure reprinted with permission from Burgess & Scott[7], copyright © 2017 Cambridge University Press.

where the subscript on $\overline{\omega_v^2}$ indicates the range.

The number density at three times compensated by $\overline{\omega_v^2}t$ is shown in figure 9. The effect on the scaling is most noticeable in range (2), where the collapse of the curves is significantly better, and the scaling range also extends to smaller scales, reflecting weak A-dependence of $\overline{\omega_v^2}$. As shown in figure 8c, the vortex number does not follow the predicted decay laws in ranges (2) and (3); instead, $N_v \sim t^{-1/3}$ and $N_v \sim t^{-2/3}$ in these ranges respectively. In contrast, $\sigma_v \sim t^{-1}$ in range (2) and $\sigma_v \sim t^0$ in range (3), as shown in figure 8d, demonstrating that the scaling theory is more properly formulated in terms of intensity-weighted vortex number σ_v rather than raw vortex number N_v. Further evidence that this is the case comes from measuring the transitional areas A_- and A_+ by fitting lines of slope -1, and -3, and -6 through the ranges and finding their intersection. The resulting transitional areas are shown in figure 10, and clearly do not follow the predictions in equation (29). Rather, $A_- \sim t^{0.659}$ and $A_+ \sim t^{1.16}$, consistent with equation (31) with $(\overline{\omega_v^2})_2 \sim t^{1/3}$ and $(\overline{\omega_v^2})_3 \sim t^{2/3}$.

Importantly, though the scaling is not clean in range 3 and the evidence for a power law is weakest at these scales, the conservation properties of this regime are clearly distinct from those of ranges 1 and 2, and are consistent with the theoretical arguments of intensity-weighted number conservation motivating equation (30). This suggests that regime 3 is dynamically distinct from ranges 1 and 2, even though power law scaling is questionable.

We note that the time-variation and weak A-dependence of $\overline{\omega_{\rm v}^2}$ are sensitive to dissipation. In particular, simulations with Laplacian (normal) viscosity, as opposed to hyperviscosity, develop vortex populations in which $\overline{\omega_{\rm v}^2}$ is time-invariant except at the largest scales[25]. In that case the number density follows (18). However, though the time-variation and area-dependence of $\overline{\omega_{\rm v}^2}$ are non-universal and depend at least on dissipation, considering these corrections to the theory has elucidated the conservation structure in the three ranges; namely $\sigma_{\rm v}$, the natural third member in the hierarchy of conserved quantities (3)–(5), and not the vortex number $N_{\rm v}$, is the correct quantity to consider in the large-scale range.

Freely evolving turbulence

In freely evolving two-dimensional turbulence the distribution of vortex intensities and the scaling of the number density are sensitive to the initial conditions[14]. As discussed above in section IIIA and shown in figure 4, top hat initial energy spectra yield distributions of intensities $\overline{\omega_{\rm v}^2}$ that vary weakly with area A and time t, in which case the number density approximately follows the prediction of equation (16). However Gaussian initial energy spectra yield intensities $\overline{\omega_{\rm v}^2}(A,t)$ that vary appreciably with A and evolve in time, as shown in figures 11a-11b. In this case, the number density no longer follows the A^{-1} law associated with a scale-invariant vortex area distribution, but rather develops two scaling ranges on either side of the area $A_{\rm p}$ at which $\overline{\omega_{\rm v}^2}$ reaches its maximum. The data are from a contour advection simulation labelled mGauss-CA on a 2048^2 basic inversion grid, with effective resolution $(16\cdot 2048)^2 = 32,768^2$, starting from an initial energy spectrum $\mathcal{E}(k) \sim k^3 e^{-2(k/k_0)^2}$, where $k_0 = 256$. Even under these conditions, an extended form of scaling holds, in which the number density compensated by the vortex intensity assumes a self-similar form

$$n(A)/\overline{\omega_{\rm v}^2}(A,t) \sim t^{-2/3} A^{-1}, \tag{32}$$

as shown in figure 11c.

Figure 12(a) shows $N_{\rm v}$, $Z_{\rm v}$, and $E_{\rm v}$ integrated over a comoving interval $[\mu A_{\rm typ}, A_{\rm typ}]$, where

$$A_{\rm typ} \equiv \frac{1}{2}\frac{\int_{A_{\rm min}}^{A_{\rm max}} \overline{\omega_{\rm v}^2} A^2 n(A) dA}{\int_{A_{\rm min}}^{A_{\rm max}} \overline{\omega_{\rm v}^2} A n(A) dA} \tag{33}$$

is an intensity-weighted 'typical' vortex area, which evolves at the mean growth rate, $A_{\rm typ} \sim t^{1/3}$, as shown in (c). The integration limits are $[A_{\rm min}, A_{\rm max}]$, where $A_{\rm min}$ and $A_{\rm max}$ are the

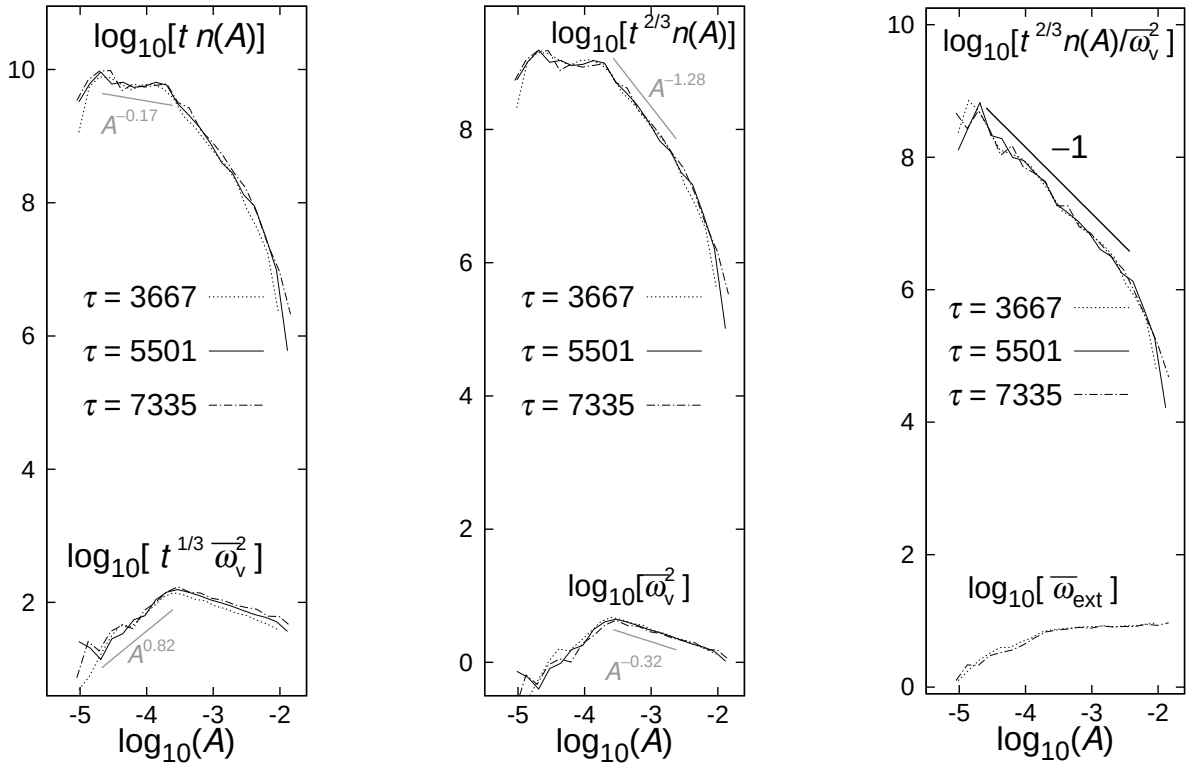

(a) (b) (c)

FIG. 11: (a)-(b) mGauss-CA vortex number density $n(A)$ and intensities $\overline{\omega_{\rm v}^2}(A,t)$ compensated by the indicated factors of t and (c) mGauss-CA number density compensated by $t^{2/3}/\overline{\omega_{\rm v}^2}$. The slopes of the scaling ranges are determined by least squares fit to be (a) (0.82 ± 0.05) and (-0.17 ± 0.05), (b) (-0.32 ± 0.01) and (-1.28 ± 0.03). Data is from a simulation described in Burgess *et al.*, "Extended scale invariance in the vortices of freely evolving two-dimensional turbulence," Phys. Rev. Fluids (Submitted).

areas of the smallest and largest vortices present at a given time. In the freely evolving system, vortex interactions generate a growing population of smaller and smaller vortices[46]; $A_{\rm min}$ is the smallest of these. The subpopulation of vortices contained in $[\mu A_{\rm typ}, A_{\rm typ}]$ follows the decay laws $N_{\rm v} \sim t^{-2/3}$, $Z_{\rm v} \sim t^{-1/3}$, and $E_{\rm v} \sim t^0$ predicted by the scale-invariant theory of Dritschel *et al.*[5], and as seen above in the A^{-1} range of simulation Tophat-PS (figure 5, left). In contrast, the vortex enstrophy decay rate in the comoving interval $[A_{\rm typ}(t), A_{\rm max}(t)]$ shown in (b) is $Z_{\rm v} \sim t^{-0.44}$. This is the global decay rate, suggesting that vortex interactions in this range of scales are predominantly responsible for coherent enstrophy decay in the system.

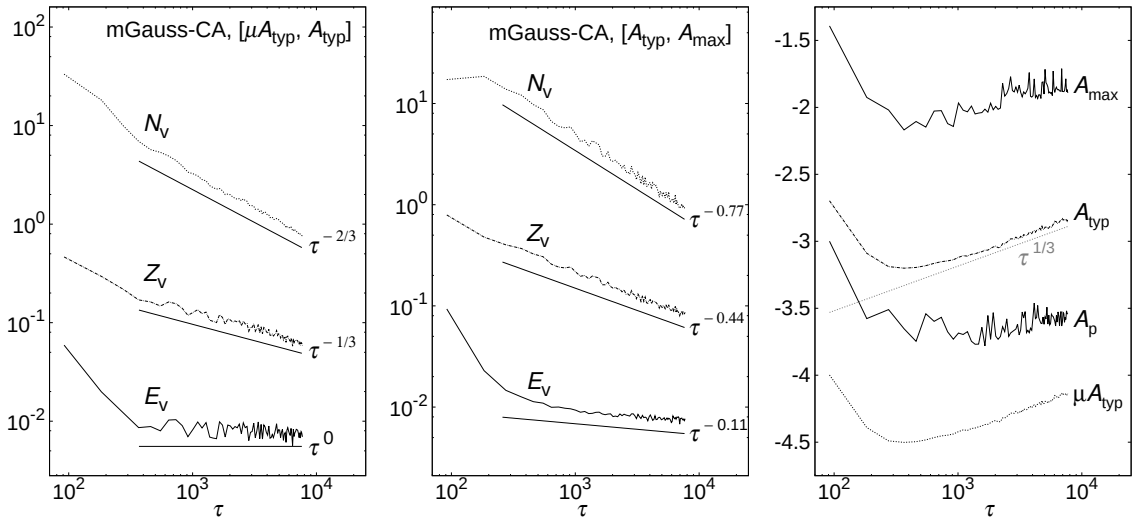

(a) (b) (c)

FIG. 12: N_v (dashed), Z_v (dash-dot), and E_v (solid) for (a) a comoving interval $[\mu A_{\rm typ}, A_{\rm typ}]$ and (b) a comoving interval $[A_{\rm typ}, A_{\rm max}]$; (c) interval endpoints, along with $A_{\rm p}$, the area at which $\overline{\omega_{\rm v}^2}(A,t)$ peaks, and $A_{\rm max}$. Data is from a simulation described in Burgess *et al.*, "Extended scale invariance in the vortices of freely evolving two-dimensional turbulence," Phys. Rev. Fluids (Submitted).

Even in simulations Tophat-CA and Tophat-PS, where the scaling of the number density is much closer to A^{-1}, compensating $n(A)$ by $t^{2/3}/\overline{\omega_{\rm v}^2}$ yields an extended scaling range with improved A^{-1} scaling, as can be seen by examining the black curves in figure 4, which show $t^{2/3}n(A)/\overline{\omega_{\rm v}^2}$ at the same three times used for the gray curves ($t^{2/3}n(A)$). The extended scaling range is marked by a -1 slope line. Least squares fits over this range yield slopes of -1.14 ± 0.05 for compensation by $t^{2/3}$ (gray curves) and -1.06 ± 0.03 for compensation by $t^{2/3}/\overline{\omega_{\rm v}^2}$ (black curves) in simulation Tophat-CA (left panel), and -1.13 ± 0.02 for compensation by $t^{2/3}$ (gray curves) and -0.99 ± 0.02 for compensation by $t^{2/3}/\overline{\omega_{\rm v}^2}$ (black curves) in simulation Tophat-PS (middle panel). This demonstrates that the extended scaling improves the scaling in this range, though interestingly not at smaller scales. Further exploration of the dependence of $n(A)$ on the initial conditions, and the regimes of validity of equation (32), will be the subject of future research.

This extended self-similar form $n(A)/\overline{\omega_{\rm v}^2} \sim t^{-2/3}A^{-1}$ preserves scale invariance in the vortex population. To see this, we consider a natural time scale associated with vortices,

the turnover time,

$$T_{\rm v} \equiv \left[\overline{\omega_{\rm v}^2}(A,t)\right]^{-1/2}, \tag{34}$$

which is a function of A, and associate with $T_{\rm v}$ a length scale $L_{\rm v}$ defined as the distance over which a vortex of area A travelling at the mean speed $u \equiv \sqrt{2E}$ completes one turnover,

$$L_{\rm v}(A,t) \equiv u\ [\overline{\omega_{\rm v}^2}(A,t)]^{-1/2}. \tag{35}$$

All vortices are assumed to travel at the same mean speed u, which holds to a very good degree in the simulations. The average intervortex distance is

$$L_{\rm r}(A,t) \equiv \left[\int_{\mu A}^{A} n(A')dA'\right]^{-1/2}, \tag{36}$$

where $0 < \mu < 1$ is a constant. Inserting the form $n(A) \sim t^{-2/3}\overline{\omega_{\rm v}^2}\omega_{\rm max}^{-2}A^{-1}$, where $\omega_{\rm max}$ is the conserved global vorticity maximum, we obtain

$$L_{\rm r}(A,t) \sim \sqrt{\frac{t^{2/3}\omega_{\rm max}^2}{\overline{\omega_{\rm v}^2}(A,t)}}. \tag{37}$$

Using this with (35) and assuming energy conservation yields

$$\frac{L_{\rm r}(A,t)}{L_{\rm v}(A,t)} \sim t^{1/3}, \tag{38}$$

such that the ratio of the average intervortex distance to the distance travelled in one turnover time is independent of scale. This is a basic requirement for self-similar vortex dynamics.

IV. CONCLUSIONS AND OUTLOOK

We have reviewed the shared mechanisms by which vortices form in both forced and freely evolving two-dimensional turbulence, merging and generating time-evolving spatial hierarchies with nontrivial spatiotemporal scaling in multiple distinct ranges. Though the original similarity theories of two-dimensional turbulence neglect vortices, they have a continued role in describing the incoherent intervortex flow. Classical similarity theories and vortex scaling theories are thus complementary, rather than in competition with each other, and together provide a more complete description of two-dimensional turbulent flows. Moreover,

as we have shown, the scaling ranges found in the vortex populations of two-dimensional turbulence can be modelled using concepts familiar from inertial range theory. Both classical inertial ranges and vortex scaling ranges can be understood as examples of fixed point solutions associated with stationary transport of conserved quantities, a generic phenomenon in far-from-equilibrium systems. In the forced system, in particular, the hierarchy of conserved quantities associated with a three-part number density provides an exciting new window into the forced inverse cascade. These findings suggest potential areas for further investigation, such as studying vortex interactions within and between the scaling ranges to understand the processes involved at different scales. Another interesting focus of research is the scale-invariant range common to forced and freely evolving vortex populations: specific questions include the extent to which the dynamics generating this range are shared between the forced and freely evolving systems, and how they are affected by the energetic background flow in the forced system. The dependence of $n(A)$, and the range of validity of the extended scaling form equation (32), also deserve further investigation. Another natural extension of this work is to three-dimensional quasi-geostrophic turbulence[47], which for constant Coriolis and buoyancy frequencies may be expected to exhibit analogous vortex scaling properties[48]. These investigations promise to yield an even more complete and unified understanding of two-dimensional turbulence and related fluid-dynamical systems.

REFERENCES

[1]R. Benzi, S. Patarnello, and P. Santangelo, "Self-similar coherent structures in two-dimensional decaying turbulence," *J. Phys. A: Math. Gen.* **21**, 1221–1237 (1988).

[2]R. Benzi, M. Collela, M. Briscolini, and P. Santangelo, "A simple point vortex model for two-dimensional decaying turbulence", *Phys. Fluids. A* **4**, 1036–1039, (1992).

[3]G. F. Carnevale, J. C. McWilliams, Y. Pomeau, J. B. Weiss, and W. R. Young, "Evolution of vortex statistics in two-dimensional turbulence", *Phys. Rev. Lett.*, **66**, 2735–2738, (1991).

[4]J. B. Weiss and J. C. McWilliams, "Temporal scaling behavior of decaying two-dimensional turbulence", *Phys. Fluids*, **5**, 608–621, (1993).

[5]D. G. Dritschel, R. K. Scott, C. Macaskill, G. A. Gottwald, and C. V. Tran, "Unifying scaling theory for vortex dynamics in two-dimensional turbulence", *Phys. Rev. Lett.*, **101**,

094501, (2008).

[6]J. Fontane, D. G. Dritschel, and R. K. Scott, "Vortical control of forced two-dimensional turbulence", *Phys. Fluids*, **25**, 015101, (2013).

[7]B. H. Burgess and R. K. Scott, "Scaling theory for vortices in the two-dimensional inverse energy cascade", *J. Fluid Mech.*, **811**, 742–756, (2017).

[8]G. K. Batchelor, "Computation of the energy spectrum in homogeneous two-dimensional turbulence," *Phys. Fluids* **12**(Suppl. 12), II-233–II-239 (1969).

[9]R. H. Kraichnan, "Inertial ranges in two-dimensional turbulence", *Phys. Fluids*, **10**, 1417–1423, (1967).

[10]B. H. Burgess, R. K. Scott, and T. G. Shepherd, "Kraichnan-Leith-Batchelor similarity theory and two-dimensional inverse cascades", *J. Fluid Mech.*, **767**, 467–496, (2015).

[11]J. C. McWilliams, "A demonstration of the suppression of turbulent cascades by coherent vortices in two-dimensional turbulence", *Phys. Fluids A*, **2**, 547–552, (1990).

[12], P. Bartello and T. Warn, "Self-similarity of decaying two-dimensional turbulence", *J. Fluid Mech.*, **326**, 357–372, (1996).

[13]J. Berges and D. Mesterhazy, "Introduction to the nonequilibrium functional renormalization group", *Nucl. Phys. B Proc. Suppl.*, **228**, 37–60, (2012).

[14]B. H. Burgess, D. G. Dritschel, and R. K. Scott, "Extended scale invariance in the vortices of freely evolving two-dimensional turbulence", *Phys. Rev. Fluids*, Submitted, (2017).

[15]P. Santangelo, R. Benzi, and B. Legras, "The generation of vortices in high-resolution, two-dimensional decaying turbulence and the influence of initial conditions on the breaking of self-similarity," *Phys. Fluids A* **1**(6), 1027–1034 (1989).

[16]J. C. McWilliams, 'The vortices of two-dimensional turbulence", *J. Fluid Mech.*, **219**, 361–385, (1990).

[17]J. C. McWilliams, "The emergence of isolated coherent vortices in turbulent flow," *J. Fluid Mech.* **146**, 21–43 (1984).

[18]R. Benzi, S. Patarnello, and P. Santangelo, "On the statistical properties of two-dimensional decaying turbulence," *Europhys. Lett.* **3**, 811–818 (1987).

[19]R. Benzi, G. Paladin, S. Patarnello, P. Santangelo, and A. Vulpiani, "Intermittency and coherent structures in two-dimensional turbulence," *J. Phys. A: Math. Gen.* **19**, 3771 (1986).

[20]A. Babiano, C. Basdevant, B. Legras, and R. Sadourny, "Vorticity and passive-scalar dynamics in two-dimensional turbulence," *J. Fluid Mech.* **183**, 379–397 (1987).

[21]L. M. Smith and V. Yakhot, "Finite-size effects in forced two-dimensional turbulence," *J. Fluid Mech.* **274**, 115–138 (1994).

[22]V. Borue, "Inverse energy cascade in stationary two-dimensional homogeneous turbulence," *Phys. Rev. Lett.* **72**, 1475–1478 (1994).

[23]R. K. Scott, "Nonrobustness of the two-dimensional turbulent inverse cascade," *Phys. Rev. E* **75**, 046301 (2007).

[24]A. Vallgren, "Infrared Reynolds number dependency of the two-dimensional inverse energy cascade," *J. Fluid Mech.* **667**, 463–473 (2011).

[25]B. H. Burgess and R. K. Scott, "Robustness of vortex populations in the two-dimensional inverse energy cascade", *J. Fluid Mech.*, Submitted, (2017).

[26]G. Haller, A. Hadjighasem, M. Farazmand, and F. Huhn, "Defining coherent vortices objectively from the vorticity", *J. Fluid Mech.*, **795**, 136–173, (2016).

[27]N. J. Zabusky, "Contour dynamics for the Euler equations in two dimensions", *J. Comp. Phys.*, **30**, 96–106, (1979).

[28]M. A. Virasoro, "Variational principle for two-dimensional incompressible hydrodynamics and quasigeostrophic flows", *Phys. Rev. Lett.*, **47**, 1181–1183, (1981).

[29]M. Roos, *Introduction to Cosmology, Fourth Edition* (Wiley, Chichester, UK, 2015).

[30]D. G. Dritschel and D. W. Waugh, "Quantification of the inelastic interaction of unequal vortices in two-dimensional vortex dynamics", *Phys. Fluids A* **4**,1737–1744 (1992).

[31]P. Tabeling, S. Burkhart, O. Cardoso, and H. Willaime, "Experimental study of two-dimensional freely decaying turbulence", *Phys. Rev. Lett.*, **67**, 3772 (1991).

[32]O. Cardoso, D. Marteau, and P. Tabeling, "Quantitative experimental study of the free decay of quasi-two-dimensional turbulence", *Phys. Rev. E*, **49**, 454 (1994).

[33]E. A. Hansen, D. Marteau, and P. Tabeling, "Two-dimensional turbulence and dispersion in a freely decaying system", *Phys. Rev. E*, **58**, 7261 (1998).

[34]A. Bracco, J. C. McWilliams, G. Murate, A. Provenzale, and J. B. Weiss, "Revisiting freely decaying two-dimensional turbulence at millenial resolution," *Phys. Fluids* **12**, 2931 (2000).

[35]A. Trizac, "A coalescence model for freely decaying two-dimensional turbulence," *Europhys. Lett.* **43**, 671 (1998).

[36]H. J. H. Clercx and A. H. Nielsen, "Vortex statistics for turbulence in a container with rigid boundaries," *Phys. Rev. Lett.* **85**, 752 (2000).

[37]C. Sire and P.-H. Chavanis, "Numerical renormalization group of vortex aggregation in two-dimensional decaying turbulence: The role of three-body interactions," *Phys. Rev. E* **61**, 6644 (2000).

[38]L. J. A. van Bokhoven, R. R. Trieling, H. J. H. Clercx, and G. J. F. van Heijst "Influence of initial conditions on decaying two-dimensional turbulence," *Phys. Fluids* **19**, 046601 (2007).

[39]G. F. Carnevale, Y. Pomeau, and W. R. Young, "Statistics of ballistic agglomeration," *Phys. Rev. Lett.* **64**, 2913 (1990).

[40]A. Trizac and J.-P. Hansen, "Dynamics and growth of particles undergoing ballistic coalescence," *J. Stat. Phys.* **82**, 1345 (1996).

[41]G. Huber and P. Alstrom, "Universal decay of vortex density in two dimensions," *Physica A* **195**, 448 (1993).

[42]Y. Pomeau, "Vortex dynamics in perfect fluids," *J. Plasma Phys.* **56**, 407 (1996).

[43]T. Iwayama, H. Fujisaka, and H. Okamoto "Phenomenological determination of scaling exponents in two-dimensional decaying turbulence," *Prog. Theor. Phys.* **98**, 1219 (1997).

[44]J. H. LaCasce "The vortex merger rate in freely decaying, two-dimensional turbulence," *Phys. Fluids* **20**, 085102 (2008).

[45]D. G. Dritschel and J. Fontane, "The combined Lagrangian advection method", *J. Comput. Phys.*, **229**, 5408–5417 (2010).

[46]D. G. Dritschel "Vortex properties of two-dimensional turbulence," *Phys. Fluids A* **5**, 984 (1993).

[47]J. G. Charney "Geostrophic turbulence," *J. Atmos. Sci.* **28**, 1087–1095 (1971).

[48]J. N. Reinaud, D. G. Dritschel, and C. R. Koudella "The shape of vortices in quasi-eostrophic turbulence," *J. Fluid Mech.* **474**, 175–192 (2003).